Evaluation of a Mutually Coupled Diversity Receiver

Christian VOLMER, Ralf STEPHAN, Matthias A. HEIN

Institute for Information Technology, Ilmenau University of Technology, P. O. Box 100565, 98684 Ilmenau, Germany

christian.volmer@tu-ilmenau.de, ralf.stephan@tu-ilmenau.de, matthias.hein@tu-ilmenau.de

Abstract. *A quick, reliable, and simple evaluation of mutual coupling effects is essential for the optimization of antenna arrays for small mobile communications devices. In recent papers we have proposed novel figures of merit that quantify the impact on diversity reception in terms of scattering matrix of the array and have confirmed the validity of these formulas by practical diversity measurements. The present paper provides an extended analysis of the measurement data and contrasts the benefits of this method of array characterization with existing approaches.*

Keywords

Mutual coupling, antenna diversity, decoupling and matching network.

1. Introduction

In order to meet the continuing demand for greater user mobility at even higher data rates, multiple antennas are employed at one or both ends of a modern mobile communications system. Since hand-held devices are expected to be small and lightweight, antenna engineers face a growing challenge of designing highly compact antenna arrays.

As the separation between radiating elements becomes smaller than half a wavelength, mutual coupling effects begin to degrade the radiation capabilities of the antenna array [1], [2]. A typical two-port design would therefore minimize the coupling coefficient s_{21} between radiators as well as the matching coefficients s_{11}, s_{22} of the individual elements. Another popular approach minimizes the correlation coefficient ρ between the signals received at the array ports.

Both approaches, however, only characterize mutual coupling itself and do not quantify the consequences specific for a communications system. In practice, the optimum condition with $s_{11} = s_{22} = 0$ and either $s_{21} = 0$ or $\rho = 0$ often cannot be attained over the desired frequency band (or bands) of operation due to space limitations. The immediate question arises of how much mutual coupling can be tolerated for a given application and to what extent correlation can be traded for matching in order to achieve an optimum design. Is there a way to characterize designs with more than two radiators? What are the possible benefits of decoupling and matching networks that attempt to eliminate the effects of mutual coupling?

To facilitate the answers to these questions, we proposed simple analytical expressions related to the performance of a diversity receiver system [3], [4] in terms of the scattering parameters of an arbitrarily coupled antenna array. The present paper summarizes these expressions, discusses their relevance to engineering applications, and elaborates on the fading measurements carried out with a three-branch diversity receiver presented in an earlier paper [5] to further substantiate their validity.

2. Diversity Figures of Merit

It is well known that the waveforms received by a mobile communications system are impaired by strong and rapid fluctuations of the signal strength. This effect is called fading. A typical diversity receiver comprises n identical receiver front-ends called "branches" followed by a combining unit. The goal is to combine the branches in a way that improves the fading statistics at the combiner output. There are various combining techniques that differ in implementation complexity and signal-to-noise ratio (SNR) performance. Maximal ratio combining (MRC) is known to deliver the maximum SNR possible at its output [6]. It seems sensible to choose the performance of a diversity receiver application as an indicator for the "quality" of a mutually coupled antenna array.

A common metric in diversity analysis is the *diversity gain* of the system with respect to some suitable non-diversity (single-antenna) system. Consider Fig. 1 where the solid graphs portray the distribution functions of the SNR of "ideal" one-, two-, and three-branch systems. They are ideal in the sense that the radiators are lossless, uncoupled, and perfectly matched, and that the communications environment is Rayleigh distributed with the directions of arrival uniformly distributed over the entire solid angle and both polarizations equally likely [3]. All graphs are normalized to the mean SNR of the single-branch system.

The y-axis reflects the probability that the instantaneous SNR drops below the mean value of 0 dB by the amount specified on the x-axis. For instance, with the single-antenna system there is a 1 % chance that the SNR fades by 20 dB or more. Additional receive antennas change the slope of the graphs in the way that deep fades become con-

siderably less likely: with the two-antenna system the chance of the same amount of fading is reduced below 0.01 %. The diversity gain G_d of a system is defined as the decibel difference of the amount of fading experienced with and without diversity at the same probability level, called the *outage probability* p. In more descriptive terms, G_d reflects the amount by which the transmit power could be reduced in a diversity application with negligible effect on system reliability and quality of service.

An example is indicated in the figure by the arrow between the single-branch and the two-branch system for a probability of $p = 1$ %. Here the diversity gain is 11.7 dB, corresponding to potential power savings of 93 % at the transmitter. The diversity gain is generally dependent on the probability level p chosen.

It was previously observed [7], [8] that, under the condition of a Rayleigh fading environment, the joint probability distribution of the received complex signal envelopes, denoted by the n-element column vector $\vec{b}$, is uniquely characterized by their complex covariance matrix

$$\mathrm{E}\left\{\vec{b}^{*}\vec{b}^{\mathrm{T}}\right\} = \tilde{H}. \tag{1}$$

In general, a number of factors affect the value of $\tilde{H}$: the angular distribution of the directions of arrival of the wavefronts impinging on the array, mutual coupling, and impedance mismatch. In addition, dissipative losses inside the antenna array, the connecting cables, or a feed network, such as a decoupling and matching network (DMN), play a major role [3], [9], [10]. The distribution functions in Fig. 1 are determined by the eigenvalues of $\tilde{H}$ and can be computed as described in [11].

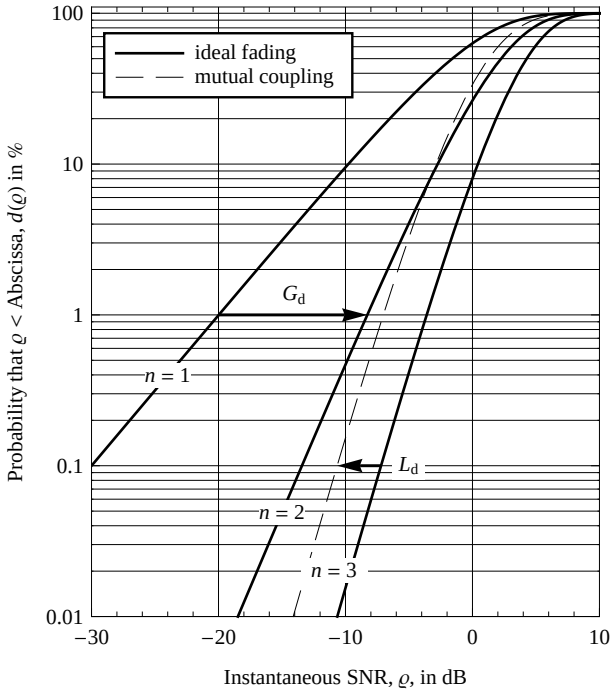

Fig. 1. Distribution functions of the combined SNR with n-branch MRC diversity reception. The solid lines represent ideal systems, the dashed line represents a three-branch system impaired by mutual coupling.

By manipulation of the distribution functions, we showed that a closed-form approximation to the diversity gain of maximal ratio combining (MRC) can be formulated in terms of $\tilde{H}$ and p [3]. Let

$$q = \sqrt[n]{n!\det\{\tilde{H}\}\,p} \tag{2}$$

where n denotes the number of array elements and $\det\{\cdot\}$ the matrix determinant. Then the diversity gain is approximately

$$G_\mathrm{d}(\tilde{H}, p) \approx \frac{q}{p}\left[1 + q\,\frac{\mathrm{tr}\{\tilde{H}^{-1}\}}{n(n+1)}\right] \tag{3}$$

where $\mathrm{tr}\{\cdot\}$ signifies the matrix trace.

In addition to the ideal diversity systems, Fig. 1 includes the theoretical distribution function of a three-branch system impaired by mutual coupling (dashed curve). It seems mutual coupling causes the graph to shift in the direction of lower SNRs with respect to the graph of ideal fading. In fact, we demonstrated that, for moderate amounts of coupling, this shift is almost parallel to the ideal graph and hence independent of the probability level p. It turns out that this *diversity loss* due to mutual coupling and impedance mismatch can be approximated by the compact expression

$$L_\mathrm{d}(\tilde{H})\Big|_\mathrm{dB} \approx -\frac{10}{n}\log\det\{\tilde{H}\}\ \mathrm{dB}. \tag{4}$$

Before we move on to the next section to discuss the different ways to establish $\tilde{H}$, we would like to point out the benefits of the above expressions. Previous designs of compact antenna arrays often aim to eliminate mutual coupling and impedance mismatch altogether and thus always result in an ideal array without need for further analysis [12], [13], [14]. Other papers concentrate on the port correlation coefficient [15], [16] or treat impedance mismatch (or the mean effective gain, MEG) as distinct quantities [1], [17], [18].

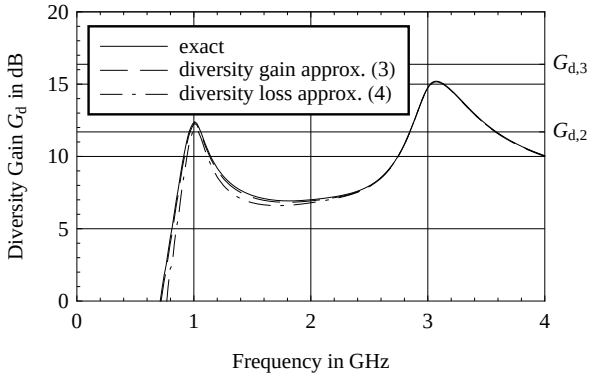

Fig. 2. Frequency sweep of the diversity gain of a 0.15λ-spaced 1 GHz dipole array. The right-hand y-axis indicates the diversity gains of ideal two- and three-element systems. Note the close agreement between the diversity gain approximation (dashed curve) and the exact graph (solid curve).

By contrast, the above figures of merit include both effects – signal correlation and impedance mismatch – in a single quantity. Provided the matrix $\tilde{H}$ is known and the environment exhibits Rayleigh-fading, different array designs can be compared immediately and unambiguously. The figures could be used as cost-functions for the parametric optimization in antenna simulation software. Another major advantage is that the formulas allow a frequency-dependent evaluation of the array properties, which is useful for the characterization of broadband or multi-band designs.

For instance, Fig. 2 plots the diversity gain of a trivial multi-band array consisting of three dipole-radiators with a separation of 0.15 λ at 1 GHz, which exploits the fact that dipoles are not only resonant at their design frequency, but also at odd multiples thereof (λ denotes the free-space wavelength). The performance difference between the two frequency bands arising from the different effective radiator separations at these frequencies is clearly evident. The graphs also convey an idea of the high accuracy of the approximation formulas proposed.

3. Signal Covariance Matrix

As stated above, fading in a Rayleigh environment is uniquely characterized by the complex covariance matrix $\tilde{H}$ of the received signal envelopes. The following subsections propose several approaches to computing $\tilde{H}$ to varying degrees of accuracy.

3.1 Uniform Rayleigh Environment

If the antenna array resides in a uniformly distributed Rayleigh environment, i.e., there is no preferred direction of arrival or polarization, and the antenna array lacks dissipative losses, then the matrix $\tilde{H}$ is a simple function of the array scattering matrix [3], [8]:

$$\tilde{H}_{\mathrm{acc}} = \tilde{I} - \tilde{S}^{\mathrm{H}}\tilde{S} \tag{5}$$

where $\tilde{I}$ is the $n \times n$ identity matrix and $^{\mathrm{H}}$ denotes the Hermitian (conjugate) matrix transpose. The subscript points out that this formula is derived by considering the power *accepted* by the antenna array, which, in the lossless case, equals the power radiated by the antenna [2]. Thus basic scattering parameter measurements or simulations suffice to obtain an initial impression of the diversity capabilities and the quality of a mutually coupled antenna array. For perfectly decoupled and matched, i.e., "ideal", antenna arrays we have $\tilde{S} = \tilde{0}$ and hence the covariance matrix equals the identity matrix.

If ohmic, i.e. dissipative, losses inside the array are of concern due to lossy antenna materials, lengthy cables, or elaborate feed structures for instance, these can be accounted for by integration over the far-field patterns of the array:

$$\tilde{H}_{\mathrm{rad},ij} = \frac{1}{4\pi}\oint \vec{F}_i^{\mathrm{H}}(\phi,\theta)\vec{F}_j(\phi,\theta)\cos\theta\,\mathrm{d}\phi\,\mathrm{d}\theta. \tag{6}$$

Here, $\vec{F}_i(\phi,\theta)$ denotes the two orthogonal polarizations of the complex embedded far-field associated with array port i dependent on azimuth ϕ and elevation θ and normalized to an isotropic radiator. All other array ports must be terminated with matched loads. The subscript "rad" signifies that this formulation is based on the power actually radiated. Appropriate far-field data are produced by most simulation software or can be obtained by calibrated antenna measurements. The diversity gain based on $\tilde{H}_{\mathrm{rad},ij}$ should be equal to the value obtained with reverberation chamber measurements [17].

3.2 Decoupling and Matching Network

We previously demonstrated the beneficial effects of decoupling and matching networks (DMN) in terms of their radiation efficiency by means of a number of compact antenna arrays whose radiator spacings had been significantly below half a wavelength [9], [10]. A DMN, which is placed between an n-port antenna array and an n-branch receiver, transforms the terminals of the antenna array into a set of ports that are uncoupled and matched. A DMN therefore possesses n input ports and n output ports. Its scattering matrix $\tilde{S}_{\mathrm{N}}$ can be written in block matrix notation as:

$$\tilde{S}_{\mathrm{N}} = \begin{pmatrix} \tilde{S}_{\mathrm{N},11} & \tilde{S}_{\mathrm{N},21}^{\mathrm{T}} \\ \tilde{S}_{\mathrm{N},21} & \tilde{S}_{\mathrm{N},22} \end{pmatrix} \tag{7}$$

where ports referred to with the index "1" are the input terminals of the network and the ports indexed "2" are connected to the antenna array. Given the scattering matrix $\tilde{S}$ and the matrix $\tilde{H}_{\mathrm{acc}}$ or $\tilde{H}_{\mathrm{rad}}$, the resulting covariance matrix $\tilde{H}_{\mathrm{S}}$ of the signal envelopes received at the newly created *system* ports can be calculated by virtue of

$$\tilde{H}_{\mathrm{S}} = \tilde{T}_{\mathrm{A}}^{\mathrm{H}}\tilde{H}\tilde{T}_{\mathrm{A}}, \quad \text{with} \quad \tilde{T}_{\mathrm{A}} = \left(\tilde{I} - \tilde{S}_{\mathrm{N},22}\,\tilde{S}\right)^{-1}\tilde{S}_{\mathrm{N},21}. \tag{8}$$

The system covariance matrix can then be substituted into (4) and (3) to account for the effects of the DMN including dissipation losses [2]. Also, the influence of a DMN on the diversity gain or loss was shown to be largely independent of the angular distribution of the environment [3].

3.3 Arbitrary Rayleigh Environment

In a uniform Rayleigh environment the shapes of the array radiation patterns are immaterial to the array's performance, as (5) suggests. Whereas the assumption of Rayleigh fading is often justified in practical scenarios lacking a line-of-sight between the participating terminals [19, Fig. 9-2-1], the assumption of a *uniform* environment is not: for an outdoor mobile satellite terminal for example, there is evidently no point in using an antenna array that is most sensitive to waves arriving in the horizontal plane. Any antenna

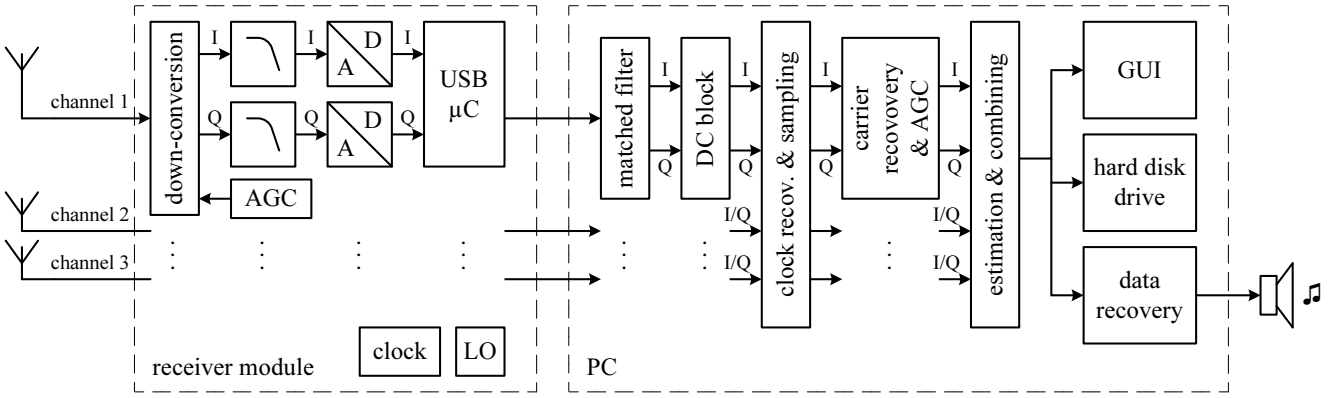

Fig. 3. Block diagram of the diversity receiver used for the fading measurements. LO = local oscillator, AGC = automatic gain control, A/D = analog-to-digital conversion, GUI = graphical user interface, PC = personal computer.

array with main beam directions pointing towards the sky clearly will be the better choice. On the other hand, the former would be an appropriate antenna for use indoors, where the wavefronts primarily impinge from around zero elevation [20].

The effects of a non-uniform environment can be accounted for by appropriate calculation of $\tilde{H}$. The diversity formulas introduced above can then be applied without modification. If the statistics of the environment are known, e.g., by channel simulation, the general formula due to Wallace and Jensen [8] should deliver the desired result. Another, simpler expression based on the popular approach by Vaughan and Bach Andersen [1] was stated in [5].

Although aspects of the environment are crucial for conclusive statements about antenna array quality and suitability with respect to a given mobile application, the measurement results presented in the next section demonstrate that the simple estimates (5) and (6) nonetheless enable accurate *relative* comparisons between arrays with similar beam-pattern characteristics in non-uniform environments. As with the effect of a DMN, it was shown that the diversity loss L_d (4) of a mutually coupled antenna array is in fact independent of the angular distribution of the environment. However, this does not hold for the diversity gain G_d.

4. Fading Measurements

In order to substantiate the practical relevance of our diversity figures of merit, we built a three-branch diversity receiver [21], which allows us to collect statistical information about the amplitudes and the phases of the received signal envelopes. A block diagram is shown in Fig. 3. After down-conversion and digitization, the baseband data are subsequently sent to a personal computer (PC) for further processing using the universal serial bus (USB) interface. The system employs quadrature phase shift keying (QPSK) as the digital modulation scheme at a symbol rate of 500 kBaud. Since the receiver has knowledge of the pseudo-random symbol sequence that is periodically broadcast by the transmitter, it can estimate the relative phase and the SNR in each branch and perform maximal ratio combining. The branch SNR data and the combined SNR data are stored to a hard disk drive for later analysis. Fig. 4 portrays a photograph of the receiver hardware.

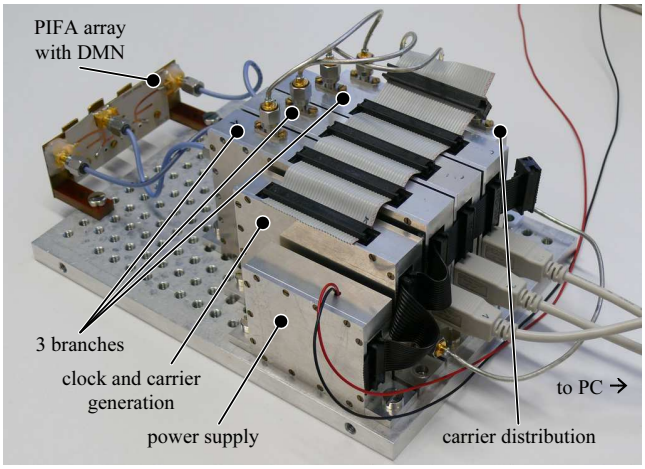

Fig. 4. Three branch diversity receiver connected to a compact three-port planar inverted-F antenna (PIFA) array with decoupling and matching network. Baseband processing is performed in real-time on a personal computer (PC).

4.1 Statistics of the Signal Strength

In a first measurement campaign, we investigated three different three-port monopole arrays with radiator separations of 0.61 λ, 0.25 λ, and 0.10 λ, respectively. A single monopole antenna was used to conduct a reference measurement. In order to imitate the environment seen by a mobile phone, where the user is allowed to turn around freely, we took twelve measurements for each array and successively rotated the array in steps of 30°. Fading was generated by moving the receiver along a seven meter hallway leading to a staircase. The transmitter was set up on the floor below

at the bottom of the staircase, without a line-of-sight to the receiver. Fig. 5 shows the measured results after normalization of the SNR data to the measured mean SNR of the single radiator. Dots indicate the measurements, the various line styles plot the theoretical CDFs based on the scattering parameters (5) of the antenna array.

Since the measured CDFs represent the average of several measurements, the figures include estimates of their standard error (estimate of the standard deviation of the mean-estimate) as error bars. The interpretation of the standard error is as follows: if the same measurement is repeated an infinite number of times, 68 % of them will likely include the true mean within the interval defined by their standard error. We must keep in mind, however, that the standard error is an estimate itself, and is based on a number of assumptions. Most notably, it requires the measurements to be repeatable and independent. Neither is true in our scenario, because the antenna arrays were rotated between measurements (i.e., the setup was changed), and because all measurements followed similar paths along the corridor (i.e., they are dependent). The error bars must therefore not be considered a rigorous statistical measure but rather an indicator for the factual deviations in a particular set of measurement data.

With the single-antenna measurement, we observe considerable differences of up to 2 dB between the measurement (thin, solid line) and the theoretical graph of Rayleigh fading. Since the theoretical graph lies far beyond the error bounds of the measurement, it is unlikely that this deviation is caused by purely random effects. A possible explanation

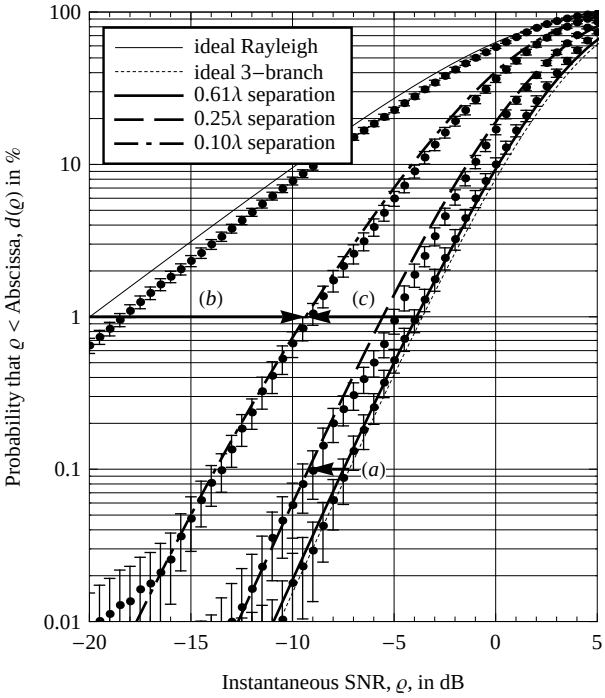

Fig. 5. Calculated and measured CDFs of linear three-port monopole antenna arrays with various radiator spacings in relation to a single monopole. The arrows indicate different diversity gains and losses with more details given in the main text.

is that the communications environment was not entirely free of a line-of-sight component so that the received SNR did not exactly follow the Rayleigh distribution. (cf. [22, Fig. 6b])

On the other hand, the plots of the three-port antenna arrays (thick lines) show remarkable agreement with the predicted distributions on a quantitative level. Although the 0.25 λ measurement deviates from the theoretical graph around $p = 1$ %, the fit is close both at the low and at the high end of the probability range. These results clearly prove the usefulness of simple scattering matrix measurements for diversity performance evaluation of mutually coupled arrays in rich multi-path environments.

Let us give some examples of the application of our diversity figures-of-merit. For the 0.25 λ array, (4) predicts a diversity loss L_d of about 2 dB, which manifests itself as a corresponding shift (arrow (a) in Fig. 5) of the CDF graph (thick, dashed line) towards lower SNRs with respect to the theoretical ideal three-port case (thin, dotted line). Note that for moderate amounts of mutual coupling, as in this example, the shift is almost parallel to the CDF of ideal three-branch diversity and hence largely independent of the probability level p.

For the 0.10 λ array, where the effects of mutual coupling are considerably more pronounced, the shift is not as much in parallel. Consequently the predicted diversity loss estimate of $L_\mathrm{d} \approx 7.4$ dB is rather pessimistic (cf. arrow (c) and (9) below); the use of the diversity loss formula (4) is therefore not recommended if mutual coupling is expected to play a dominant role in an antenna array design (cf. [3]).

The diversity gain formula (3), on the other hand, predicts a gain of $G_\mathrm{d} = 10.3$ dB for the 0.10 λ array at the 1 % probability level (thick, dash-dot line, arrow (b)). This is clearly reflected by the measurement, at least with respect to the theoretical graph of single radiator fading. Even if we decide not to rely on the absolute diversity gain measure due to the large discrepancy of the single-radiator measurement, the diversity gain formula (3) nonetheless allows a more accurate estimation of the diversity loss relative to the ideal three-port system. For instance, at $p = 1$ % we obtain

$$L_\mathrm{d}\Big|_\mathrm{dB} \approx \frac{G_\mathrm{d} \text{ of ideal array}}{G_\mathrm{d} \text{ of .0 λ array}}\Big|_\mathrm{dB} = 6.0 \text{ dB}, \qquad (9)$$

which is in excellent agreement with the measurements and indicated by arrow (c) in the figure.

Observe that even the 0.61 λ array displays some amount of coupling, which is apparent in both the theoretic CDF graph as well as the measurement. The corresponding diversity loss estimate is 0.3 dB.

In order to verify the formulas of Section 3.2, which account for a decoupling and matching network (DMN), measurements of a $\lambda/20$-spaced two-port monopole array, without and with DMN, were carried out. The DMN, which is depicted in Fig. 6, is based on the popular hybrid coupler

method described in [2], [23], because it is particularly simple to manufacture as a microstrip transmission line network. The scattering matrix $\tilde{S}$ of the antenna array was measured directly; the scattering matrix $\tilde{S}_N$ of the DMN and hence the matrix $\tilde{T}_A$ in (8) were obtained by simulation in a planar electromagnetic simulator that takes account of substrate and conductor losses [24].

The measurement results are reported in Fig. 7. When we compare the single-antenna reference measurements of Fig. 7 and Fig. 5, which were both conducted in the same environment, we observe that the second measurement lies closer to the theoretical Rayleigh graph than the previous one. However, the discrepancy again cannot be explained by the estimated standard error and this observation supports our previous suspicion that the environment may not have been completely free of a line-of-sight component.

The graphs of the antenna arrays, on the other hand, raise doubts as to the expressiveness of the standard error. Both measurements employed the same radiating structure; the only difference was the absence or presence of a DMN, which should manifest itself as a mere horizontal shift in the graphs, as pointed out at the end of Section 3.2. However, both graphs exhibit significant deviations from the theoretical CDF in *opposing* directions, yet this is not accounted for by the magnitude of the standard error. The inter-quartile range (not shown) of the acquired data shows similar behaviour: strong bias away from the theory, but no indication that the measurements are especially uncertain in the region of interest. Aside from purely random variations, it seems additional factors affect the quality of the measurements. These may include the position of the person operating the trolley carrying the receiver hardware (although it was attempted to minimize the effect) and the path along the corridor chosen.

The additional diversity gain brought about by the

Fig. 6. Two-element monopole array with a radiator separation of $\lambda/20$ at 2.45 GHz. The right-hand side photograph shows the hybrid-coupler based decoupling and matching network mounted to the rear of the ground plane.

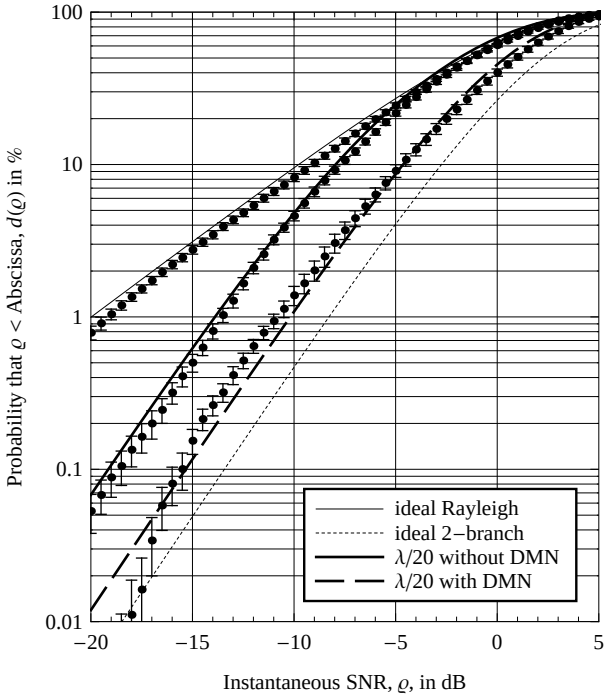

Fig. 7. Calculated and measured CDFs for the $\lambda/20$ two-port monopole array of Fig. 6 without and with DMN in relation to a single monopole.

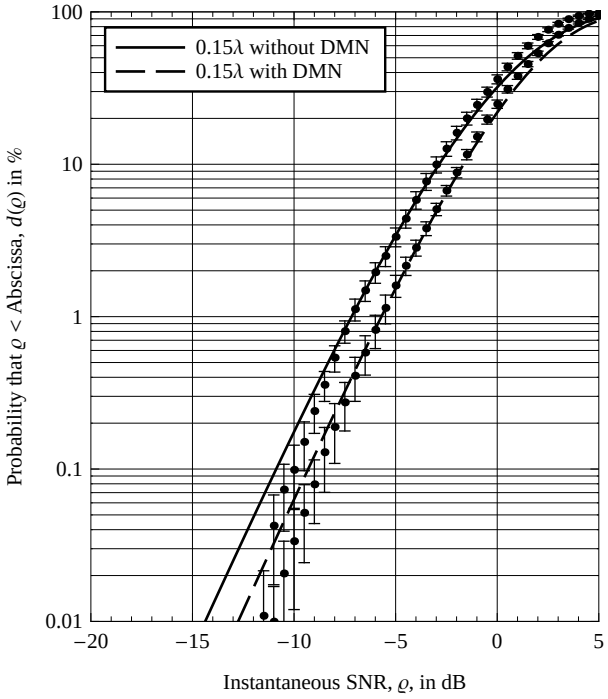

Fig. 8. Calculated and measured CDFs for the 0.15 λ three-port planar inverted-F antenna (PIFA) array of Fig. 9 without and with DMN. There is no reference measurement.

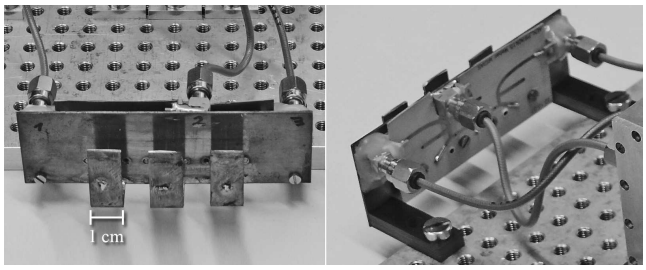

Fig. 9. Photograph of the PIFA array with decoupling and matching network. This array was designed by Weber [25].

DMN is 3.9 dB as predicted by (4), which agrees with the measurement given the remaining uncertainty in the graphs. The example demonstrates that the proposed figures of merit are not only useful for the characterisation of mutually coupled antenna arrays themselves but also predict the benefits due to a DMN based on simulated network data.

One last example is presented in Fig. 8 where the performances of planar inverted-F antenna arrays (PIFA array, photograph see Fig. 9) without and with DMN are compared. Since no reliable scattering parameters of the DMN were available, the theoretical plots are based on the matrix $\tilde{H}_{\text{rad}}$, i.e., on the measured far-field patterns of the array (see (6)). Apart from deviations at lower probability levels, the agreement with the predicted graphs is excellent. The diversity gain due to the DMN is about 1.7 dB according to both the measurements and the theory.

In summary, the above results demonstrate a number of important aspects of diversity reception with compact arrays. They show the severe negative impact of mutual radiator coupling on the received signal strength and verify the beneficial effects of decoupling and matching networks in the context of a practical receiver system. Most importantly, they reveal the close consistency between the theoretically predicted and the measured SNR distributions in a realistic communications scenario, and thus emphasize the practical value of the diversity figures of merit introduced in this paper.

4.2 Covariance Matrix Estimation

The CDF graphs are not the only information we can extract from the acquired baseband data. Knowing the received signal SNR in both amplitude and phase essentially means knowing the complex received signal envelope vector $\vec{b}$ introduced in (1) up to a constant factor. The received signal covariance matrix $\tilde{H}_{\text{meas}}$ is then estimated by approximation of the expectation operator via the sample mean, i.e.,

$$\tilde{H}_{\text{meas}} = \mathrm{E}\left\{\vec{b}^{\mathrm{T}}\,\vec{b}^{*}\right\} \approx \frac{1}{N}\sum_{k=1}^{N}\vec{b}^{\mathrm{T}}[k]\,\vec{b}^{*}[k]. \qquad (10)$$

The sample index is denoted by k, and N is the total number of samples recorded. For comparison with the theory, the estimated covariance matrix $\tilde{H}_{\text{meas}}$ is normalized to the mean received power of the corresponding single-radiator measurement.

Tab. 1 summarizes the diversity losses (4) predicted from the matrices $\tilde{H}_{\text{acc}} = \tilde{I} - \tilde{S}^{\mathrm{H}}\tilde{S}$ or $\tilde{H}_{\text{rad}}$ (for the PIFA arrays) in comparison with the values obtained from the measurement-based matrices $\tilde{H}_{\text{meas}}$. The numbers in the table are derived from the same sets of data as the CDF plots of the previous section. The estimated standard error is also shown and is mostly below 0.3 dB.

The maximum difference between measured and predicted diversity loss is with the decoupled and matched $\lambda/20$ array and amounts to about 0.65 dB. This corresponds to an uncertainty in the linear diversity loss of around 16 %. The disagreement between most pairs of values again cannot be explained by the standard error alone. On the one hand, most measured diversity losses are smaller compared with the theoretical ones, i.e., according to the measurement most arrays perform better than predicted. On the other hand, this is in contrast to the CDF graphs, where, strictly speaking, the measured arrays perform worse than predicted when compared with the *single-radiator* measurement. Furthermore, given that the influence of a DMN ought to be independent of the communications environment, the measurements of the $\lambda/20$ and the PIFA array strongly suggest that the error is non-systematic: whereas the measured and the predicted DMN gains show excellent agreement for the $\lambda/20$ array, the discrepancy is rather large for the PIFA array. Judging by the corresponding CDF graphs, though, we would probably consider the PIFA measurement more accurate than the $\lambda/20$ measurement.

Since it is the eigenvalues of $\tilde{H}$ that ultimately determine diversity performance [7], a comparison between the measured and the predicted data is reported in Tab. 2. While generally the data agree fairly well, there are notable incon-

Antenna array	**— Diversity Loss, L_{d}, in dB —**		
under test	**Prediction**	**Measurement**	**Difference**
3-port, 0.61λ	0.29	0.38 ± 0.12	-0.086
3-port, 0.25λ	2.1	1.7 ± 0.12	0.39
3-port, 0.10λ	7.5	7.0 ± 0.15	0.49
$\lambda/20$ w/o DMN	5.8	5.3 ± 0.22	0.50
$\lambda/20$ w/ DMN	1.9	1.3 ± 0.20	**0.65**
DMN gain:	3.9	4.1 ± 0.30	-0.14
PIFA w/o DMN	3.8	3.5 ± 0.16	0.31
PIFA w/ DMN	2.1	2.3 ± 0.083	-0.15
DMN gain:	1.7	1.2 ± 0.18	0.46

Tab. 1. Overview of the diversity loss L_{d} as calculated from the matrix $\tilde{H}_{\text{acc}} = \tilde{I} - \tilde{S}^{\mathrm{H}}\tilde{S}$ or $\tilde{H}_{\text{rad}}$ (for the PIFA array) and the covariance matrix $\tilde{H}_{\text{meas}}$ estimated from the measured envelope data. The measured values include the estimated standard error.

Antenna array under test	— Eigenvalues — Prediction	Measurement	Standard error
3-port, 0.61λ	0.97 0.94 0.89	1.1 0.90 0.82	0.13 0.035 0.038
3-port, 0.25λ	0.95 0.94 **0.27**	0.96 0.83 **0.40**	0.048 0.015 0.025
3-port, 0.10λ	0.87 0.57 0.012	0.90 0.66 0.014	0.039 0.055 0.00087
λ/20 w/o DMN	0.93 0.074	1.1 0.078	0.055 0.0081
λ/20 w/ DMN	0.79 0.52	0.86 0.65	0.058 0.051
PIFA w/o DMN	0.77 0.74 **0.13**	0.63 0.57 **0.25**	0.038 0.024 0.019
PIFA w/ DMN	0.74 0.70 0.45	0.84 0.56 0.45	0.062 0.037 0.017

Tab. 2. Overview of the eigenvalues of the predicted covariance matrix $\tilde{H}_{\text{acc}} = \tilde{I} - \tilde{S}^{\text{H}}\tilde{S}$ or $\tilde{H}_{\text{rad}}$ (for the PIFA array) and the measured covariance matrix $\tilde{H}_{\text{meas}}$. The measured values include the estimated standard error.

sistencies, particularly with the PIFA arrays. Without DMN the smallest eigenvalue of the measurement is almost twice the prediction, whereas with DMN these values conform exactly, although both arrays only differ in their feed network. Similar contradictions exist between the 0.25 λ and the 0.10 λ array and in fact between all arrays, albeit to a far lesser extent.

5. Conclusion

We can conclude that the observed deviations both in the envelope covariance matrix as well as in the CDF graphs cannot be explained by statistical uncertainty alone. Yet the errors seem arbitrary and in this way do not suggest a general and reproducible bias in the diversity theory or the formulas derived from it. Instead, the measurements manifestly support the practical applicability of scattering parameter measurements for the evaluation of the diversity performance of mutually coupled antenna arrays. This applies to the effects of the antenna arrays themselves as well as to the evaluation of DMNs based on simulated network data.

On a final note, we must keep in mind that, between measurements, the antenna arrays were rotated in order to achieve a uniform power distribution in the azimuth plane. The elevation angle, on the other hand, certainly experienced a non-uniform power profile, which violates the basic prerequisite of the diversity gain and loss formulas. The measurements nonetheless conform well to the theory. The reason is that we compare antennas and antenna arrays that exhibit similar far-field characteristics and thus similar focusing properties over elevation. That is, monopole arrays are compared with a monopole antenna and the PIFA array is compared with itself without and with DMN. If we investigated the performances of antenna arrays with greatly differing focusing properties, we could expect considerable disagreements. The reason why no comparison between the PIFA and the monopole arrays is given at this point is because the measurements were carried out on different days and no reference data for the PIFA is available. The techniques discussed in Section 3.3 can be included in the diversity analysis if the angular distribution and the polarization characteristics of the environment are to be taken into account.

Acknowledgements

The authors gratefully acknowledge the Space Agency of the German Aerospace Center DLR (grant no. 50YB0509) for financial support on behalf of the German Federal Ministry of Economics and Technology. Special mention deserve our student assistants C. Großmann and U. Wetzker. Without their engagement and skills in USB and FPGA development this publication would not exist. Technical assistance by M. Zocher and M. Huhn is highly appreciated.

References

[1] VAUGHAN, R. G. BACH ANDERSEN, J. Antenna diversity in mobile communications. *IEEE Transactions on Vehicular Technology*, 1987, vol. 36, no. 4, p. 149–172.

[2] VOLMER, C., WEBER, J., STEPHAN, R., BLAU, K., HEIN, M. A. An eigen-analysis of compact antenna arrays and its application to port decoupling. *IEEE Transactions on Antennas and Propagation*, 2008, vol. 56, no. 2, p. 360–370.

[3] VOLMER, C., WEBER, J., STEPHAN, R., HEIN, M. A. A descriptive model for analyzing the diversity performance of compact antenna arrays. *IEEE Transactions on Antennas and Propagation*, 2009, vol. 57, no. 2, p. 395–405.

[4] VOLMER, C. *Compact Antenna Arrays in Mobile Communications: a Quantitative Analysis of Radiator Coupling*. Ph.D. dissertation. Ilmenau (Germany): Ilmenau University of Technology. In preparation.

[5] VOLMER, C., WEBER, J., STEPHAN, R., HEIN, M. A. Mutual coupling in multi-antenna systems: Figures-of-merit and practical verification. In *Proc. 3rd Eur. Conf. Antennas Propag. (EuCAP)*. Berlin (Germany), 2009.

[6] BRENNAN, D. G. Linear diversity combining techniques. *Proc. IRE*, 1959, vol. 47, no. 6, p. 1075–1102.

[7] PIERCE, J. N. STEIN, S. Multiple diversity with nonindependent fading. *Proc. IRE*, 1960, vol. 48, no. 1, p. 89–104.

[8] WALLACE, J. W. JENSEN, M. A. Termination-dependent diversity performance of coupled antennas: Network theory analysis. *IEEE Transactions on Antennas and Propagation*, 2004, vol. 52, no. 1, p. 98–105.

[9] WEBER, J., VOLMER, C., BLAU, K., STEPHAN, R., HEIN, M. A. Miniaturized antenna arrays with an element separation down to $\lambda/10$. In *Proc. IEEE International Symposium on Antennas and Propagation (APS)*. Honolulu (USA), 2007.

[10] WEBER, J., VOLMER, C., STEPHAN, R., HEIN, M. A. Eigenmode decoupling of miniaturised diversity antennas using compact quasi-lumped networks. In *Proceedings of Loughborough Antennas and Propagation Conference (LAPC)*. Loughborough (UK), 2008.

[11] NØRKLIT, O., TEAL, P. D., VAUGHAN, R. G. Measurement and evaluation of multi-antenna handsets in indoor mobile communication. *IEEE Transactions on Antennas and Propagation*, 2001, vol. 49, no. 3, p. 429–437.

[12] CHIAU, C. C., CHEN, X., PARINI, C. G. A compact four-element diversity-antenna array for PDA terminals in a MIMO system. *Microwave and Optical Technology Letters*, 2005, vol. 44, no. 5, p. 408–412.

[13] DIALLO, A., LUXEY, C., LE THUC, P., STARAJ, R., KOSSIAVAS, G. Study and reduction of the mutual coupling between two mobile phone PIFAs operating in the DCS1800 and UMTS bands. *IEEE Transactions on Antennas and Propagation*, 2006, vol. 54, no. 11, p. 3063–3074.

[14] NILSSON, A., BODLUND, P., STJERNMAN, A., JOHANSSON, M., DERNERYD, A. Compensation network for optimizing antenna system for MIMO application. In *Proceedings of 2nd European Conference on Antennas and Propagation (EuCAP)*. Edinburgh (UK), 2007.

[15] REMBOLD, B. Relation between diagram correlation factors and S-parameters of multiport antenna with arbitrary feeding network. *Electron. Lett.*, vol. 44, no. 1, p. 5–7, Jan. 2008.

[16] DOSSCHE, S., ROMEU, J., BLANCH, S. Decoupling and decorrelation of two closely spaced monopoles for optimum MIMO capacity. In *Proceeding of 1st European Conference on Antennas and Propagation (EuCAP)*. Nice (France), 2006.

[17] KILDAL, P.-S. ROSENGREN, K. Correlation and capacity of MIMO systems and mutual coupling, radiation efficiency, and diversity gain of their antennas: Simulations and measurements in a reverberation chamber. *IEEE Commununication Magazine*, 2004, vol. 42, no. 12, p. 104–112.

[18] LAU, B. K., BACH ANDERSEN, J., KRISTENSSON, G., MOLISCH, A. F. Impact of matching network on bandwidth of compact antenna arrays. *IEEE Transactions on Antennas and Propagation*, 2009, vol. 54, no. 11, p. 3225–3238.

[19] SCHWARTZ, M., BENNETT, W. R., STEIN, S. *Communication Systems and Techniques*. 1st ed. New York: McGraw-Hill, 1966.

[20] MEDBO, J. BERG, J.-E. Spatio-temporal channel characteristics at 5 GHz in a typical office environment. In *Proceedings of 54th IEEE Vehicular Technology Conference (VTC), vol. 3*. Atlantic City (USA), 2001, p. 1256–1260.

[21] VOLMER, C., WEBER, J., STEPHAN, R., HEIN, M. A. Performance measurements of a two-branch diversity receiver with superdirective antenna array and decoupling and matching network. In *Proceedings IEEE International Symposium on Antennas and Propagation (APS)*. San Diego (USA), 2008.

[22] DIETRICH, JR., C. B., DIETZE, K., NEALY, J. R., STUTZMAN, W. L. Spatial, polarization, and pattern diversity for wireless handheld terminals. *IEEE Transactions on Antennas and Propagation*, 2001, vol. 49, no. 9, p. 1271–1281.

[23] LEE, T.-I. WANG, Y. E. A mode-based supergain approach with closely coupled monopole pair. In *IEEE MTT-S International Microwave Symposium Digest*. Los Angeles (USA), 2007.

[24] Advanced Design System (ADS). Agilent Technologies, 395 Page Mill Road, Palo Alto, CA 94304, USA.

[25] WEBER, J. *Entwurf miniaturisierter Antennengruppen*. Ph.D. dissertation. Ilmenau (Germany): Ilmenau University of Technology, 2009. in German, in press.

About Authors...

Christian VOLMER received the Dipl.-Ing. degree (with distinction) in electrical engineering and information technology from Ilmenau University of Technology, Ilmenau, Germany, in 2005, where he is currently conducting a research project funded by the German Ministry for Education and Research on mobile satellite communication system operating in the Ka-band.

Ralf STEPHAN was born in Erfurt, Germany, in 1959. He received the Dipl.-Ing. and the Dr.-Ing. degrees in theoretical electrical engineering from Ilmenau University of Technology, Ilmenau, Germany, in 1982 and 1987, respectively. From 1982 to 1989, he worked in the field of RF semiconductor modeling and circuit analysis. In 1987, he joined the Microwave Department, Ilmenau University of Technology. His research interests include modeling of microwave circuits and systems, antenna technology and EM field analysis.

Matthias A. HEIN received the diploma and doctoral degree with honors from the Bergische Universität Wuppertal, Germany, in 1987 and 1992, respectively. While at the Bergische Universität Wuppertal, he was involved in the development of superconductors for microwave applications, e.g., in mobile communications and satellite systems. In 1999, he received a British Senior Research Fellowship of the EPSRC at the University of Birmingham, Birmingham, U.K. From 1998 until 2001, he headed an interdisciplinary research group of applied physics and electrical engineering, focusing on the microwave engineering of passive microwave devices and SQUIDs. His Habilitation thesis was published as a monograph of the Springer Tracts of Modern Physics.He has authored and coauthored about 200 publications or proceedings, provided more than 30 invited talks and gave three lecture courses or tutorials at international conferences. He acts as a referee for eight high-ranking scientific journals and international funding agencies. In 2002, he joined Ilmenau University of Technology, where he now heads the RF and Microwaves Research Laboratory. His research is focused on novel microwave concepts, e.g., for antennas, amplifiers, and sensors, and microwave technologies, e.g., ceramic multilayers and MEMS (see http://www.tu-ilmenau.de/hmt).